ISSN 0021-8944, Journal of Applied Mechanics and Technical Physics, 2015, Vol. 56, No. 3, pp. 454–463. © Pleiades Publishing, Ltd., 2015.
Original Russian Text © Y. Shekari, M. Javan, A. Eghbalzadeh.

EFFECT OF TURBULENCE MODELS ON THE SUBMERGED HYDRAULIC JUMP SIMULATION

Y. Shekari[a], M. Javan[b], and A. Eghbalzadeh[b]

UDC 532.53

Abstract: This study presents a numerical investigation and prediction of the flow field in three-dimensional submerged hydraulic jumps. The volume of fluid (VOF) method is used to simulate the free surface. The turbulent structure is simulated by using different turbulence models, such as the standard k–ε model, RNG k–ε model, realizable k–ε model, and Reynolds-stress model (RSM) closure schemes. The capabilities of the turbulence models are investigated with the standard wall functions and enhanced wall treatment methods. A comparison between the numerical and experimental results shows that the numerical model is adequate for predicting the flow pattern and free surface of submerged hydraulic jumps. The RNG k–ε turbulence model with the enhanced wall treatment method ensures the highest accuracy in the water surface simulation. Near the channel bed of a fully developed region, the RSM model with the enhanced wall treatment method shows better agreement with the experimental longitudinal velocity than the other turbulence models. The standard k–ε model predicts the longitudinal velocity more accurately than the RNG and realizable k–ε models.

Keywords: three-dimensional numerical simulation, submerged hydraulic jump, turbulence model, near-wall treatment.

DOI: 10.1134/S0021894415030153

INTRODUCTION

The transition from a supercritical flow to a subcritical flow with intense turbulent mixing and air bubble entrainment is regarded as a hydraulic jump. In an open channel, when a hydraulic jump occurs, the velocity-dependent flow depth rapidly changes within a relatively short distance. In submerged hydraulic jumps, the flow transition region is located under the water surface. Free and submerged hydraulic jumps have been extensively studied due to their engineering applications.

The classic hydraulic jumps in a horizontal and wide rectangular channel with a smooth bed have been extensively studied [1–5]. Under specific conditions, the dissipation of the energy in a submerged jump might be less than that in a free jump [6]. The velocity profiles below the roller, for both submerged and free jumps, resemble those of a turbulent wall jet under an adverse pressure gradient [7]. Comparisons between free jumps, submerged jumps, and wall jets structures showed that submerged jumps could be regarded as a transition between wall jets and free jumps [8]. The experimental studies [9] indicated that the submerged jump is three-dimensional in nature. Investigations on submerged hydraulic jumps below abrupt expansions showed that both symmetric and asymmetric flows can be formed under special hydraulic conditions. Relations for determining the main submerged jump characteristics below abrupt expansions were provided [10]. The turbulence structure of a submerged hydraulic jump in a rectangular channel with horizontal rough beds was experimentally investigated [11].

[a]Department of Civil Engineering, Razi University, Kermanshah, Iran. [b]Department of Civil Engineering, Razi University–Water and Wastewater Research Center, Razi University, Kermanshah, Iran; yones.shekari@yahoo.com; javanmi@gmail.com; eghbalzadeh@gmail.com. Translated from Prikladnaya Mekhanika i Tekhnicheskaya Fizika, Vol. 56, No. 3, pp. 128–138, May–June, 2015. Original article submitted July 29, 2013.

During the past few decades, numerical methods are capable of analyzing complex problems in various sciences, especially in hydraulic engineering, for example, a two-dimensional model developed by using the standard k–ε model for simulating submerged hydraulic jumps below a sluice gate [12]. Supercritical and subcritical flows and a free hydraulic jump in a rectangular channel with a low bed slope were numerically simulated by applying the Boussinesq equations [13]. A free hydraulic jump with a non-hydrostatic pressure assumption was numerically investigated [14]. Ma et al. [15] developed a two-dimensional model for simulation of a submerged hydraulic jump by the standard k–ε turbulence model and the volume of fluid (VOF) method [16]. They demonstrated that wall functions may not be applicable to the boundary layer flow regions of a submerged hydraulic jump. Numerical simulations of a free hydraulic jump by the RNG k–ε turbulence model and the VOF method were performed in [17]. A numerical study of a free hydraulic jump by the k–ε turbulence model was conducted in [18]. A free hydraulic jump on a smooth bed was studied by using the k–ε turbulence model and large eddy simulation (LES) in [19].

In this study, the effects of the turbulence models, such as the Reynolds stress model (RSM), standard k–ε, RNG k–ε, and realizable k–ε turbulence models, on the flow structure of a submerged hydraulic jump are investigated. In addition, the performance of these turbulence models with the standard wall functions [20] and enhanced wall treatment method [21–24] is studied.

1. GOVERNING EQUATIONS

The flow field is calculated by the continuity equation and unsteady Reynolds-averaged Navier–Stokes (RANS) equations:

$$\frac{\partial(\rho u_i)}{\partial x_i} = 0,$$

$$\frac{\partial(\rho u_i)}{\partial t} + \frac{\partial(\rho u_i u_j)}{\partial x_j} = -\frac{\partial p}{\partial x_i} + \frac{\partial}{\partial x_j}\mu\Big(\frac{\partial u_i}{\partial x_j} + \frac{\partial u_j}{\partial x_i}\Big) + \frac{\partial(-\rho\overline{u_i' u_j'})}{\partial x_j}.$$

In these equations, u_i, u_j $(i, j = 1, 2, 3)$, p, ρ, μ, and $\rho\overline{u_i' u_j'}$ are the average velocity components in Cartesian coordinates, pressure, density, dynamic viscosity, and Reynolds stresses, respectively. Turbulent flows can be simulated by using various turbulence models. In this study, the commercial software is used to solve the governing equations and to simulate a three-dimensional submerged hydraulic jump. The QUICK and first-order upwind schemes are used for solving the momentum and turbulence equations, respectively. The PRESTO scheme and the PISO algorithm are applied, respectively, to discretize the pressure gradient and to couple the pressure and velocity. For solving the unsteady flow equations, the time step is set equal to 0.01 s. The governing equations are solved until their normalized residuals are equal to or smaller than 10^{-4}.

2. GRID LAYOUT

Three experiments conducted by Long et al. [9] are used to validate the numerical model. Long et al. [9] performed their experiments in a rectangular channel whose width was $Z = 0.467$ m; the channel was 7.5 m long and 0.515 m deep. Table 1 shows the primary details of the experiments selected in the present study (Y_2, Y_t, Y_1, and U_1 are the free jump depth, downstream tail water depth, inlet opening of the gate, and average inlet velocity, respectively). The submergence factor S and the inlet Froude number Fr_1 are defined by $S = (Y_t - Y_2)/Y_2$ and $\mathrm{Fr}_1 = U_1/\sqrt{gY_1}$.

3. DISCRETIZATION OF THE COMPUTATIONAL DOMAIN

Due to the axial symmetry of the experimental flow field, the half width of the channel is simulated for decreasing the computational time. The non-uniform grid is fine enough near the gate because of the rapid variation

Table 1. Primary details of experiments selected for numerical simulations

Experiment number	Y_1, m	U_1, m/s	Y_2, m	Y_t, m	Fr_1	S
3	0.025	1.58	0.10	0.187	3.19	0.85
6	0.025	2.72	0.18	0.299	5.49	0.63
8	0.015	3.14	0.17	0.206	8.19	0.24

Table 2. Grid nodes

Near-wall treatment approach	Grid nodes	
	Experiment Nos. 3 and 6	Experiment No. 8
Standard wall functions	$281 \times 38 \times 15$	$281 \times 35 \times 15$
Enhanced wall treatment	$281 \times 45 \times 33$	$281 \times 41 \times 33$

in the flow field and free surface of the roller region. The standard wall functions and the enhanced wall treatment method are used to investigate the wall effects on the flow structure. In the standard wall functions, the first node must be located in the region $y^+ > 30$ (y^+ is the dimensionless wall distance). Due to resolving the viscosity-affected near-wall region in the enhanced wall treatment method, the finest mesh in the viscous sublayer is needed, and the first grid point must be located in the region $y^+ \approx 1$. Table 2 shows the grid nodes in these numerical simulations.

4. BOUNDARY CONDITIONS

The boundary conditions of the computational domain are considered as the experimental setup. At the inlet boundary, the vertical distribution of the longitudinal velocity u measured in [9] is $u/U_1 = 0.99 + 0.02y/Y_1$. The maximum decrease in the longitudinal velocity at the gate opening is 2 to 6%.

The turbulent kinetic energy k and its dissipation rate ε at the gate opening boundary are specified as follows [9]:

$$k = 1.4 \cdot 10^{-3} U_1^2, \qquad \varepsilon = 2.2 \cdot 10^{-5} U_1^3 / Y_1.$$

The RANS simulation results (such as k–ε model predictions) depend on adequate near-wall treatment [25–27]. Therefore, different wall treatment methods, such as the standard wall functions and enhanced wall treatment, are considered for modeling the bed and the side wall.

The wall functions established for a fully developed flow region are applied to bridge the viscous sublayer region between the wall and the fully turbulent region. As the viscous sublayer and the buffer layer region are not fully resolved, the use of a very fine near-wall mesh could be avoided [20]. On the other hand, the near-wall region is totally resolved in the enhanced wall treatment method, where a very fine near-wall mesh must be used. Thus, the enhanced wall treatment method is more appropriate for complex near-wall flows [21–23, 25]. The pressure outlet and symmetry boundary conditions are applied to the outlet and symmetry planes of the channel, respectively. At the outlet boundary, the water elevation is set equal to the measured tail water depth.

5. RESULTS AND DISCUSSION

Submerged hydraulic jumps can be divided into the developing, fully developed, and recovering regions [12]. If the roller length is defined as the length of the submerged jump, 15 and 85% of the jump length are located in the developing and fully developed regions, respectively. The effects of the roller region are eliminated in the recovering region [9]. The present numerical simulations are verified by the experimental results of Long et al. [9]. The relative root-mean-square error (RMSE) Δ is calculated as

$$\Delta = \left(\frac{1}{N} \sum_{i=1}^{N} (e_{i,e} - e_{i,c})^2 \right)^{1/2} \cdot 100.$$

Here N is the number of measured points and $e_{i,e}$ and $e_{i,c}$ are the experimental and calculated values at the point i, respectively.

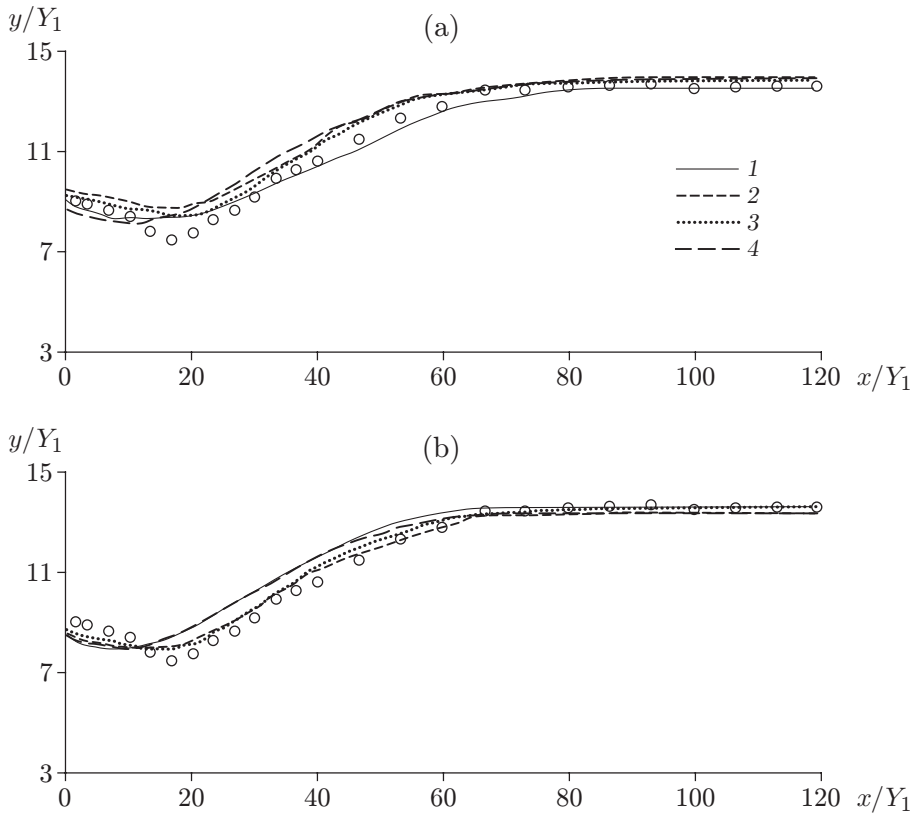

Fig. 1. Calculated (curves) and experimental (points) profiles of the water surface: (a) simulations by the standard wall functions; (b) simulations with the enhanced wall treatment; points *1–4* are obtained with the use of the RSM, standard k–ε, RNG k–ε, and realizable k–ε models, respectively; the points are the experimental data [9] (experiment No. 8).

Table 3. Relative root-mean-square error of the simulated water surface profiles

Near-wall treatment approach	Turbulence model	Δ, %
Standard wall functions	RSM	0.50
	RNG k–ε model	0.63
	Realizable k–ε model	0.93
	Standard k–ε model	0.90
Enhanced wall treatment	RSM	0.99
	RNG k–ε model	0.47
	Realizable k–ε model	0.54
	Standard k–ε model	0.99

The water surface and longitudinal velocity profiles of experiment No. 8 were simulated and compared with the experimental values in Figs. 1 and 2. The near-wall treatments and turbulence models affect the simulated water surface profiles. According to the RMSEs in Table 3, the best prediction of the water surface profile is provided by the enhanced wall treatment method and the RNG k–ε turbulence model, and the RSM with the standard wall functions is the second best in terms of the water surface prediction.

The agreement between the numerical and experimental results is excellent in the wall jet region (see Fig. 2). However, in the reverse flow, the velocity simulated by all the near wall treatments and turbulence models is slightly overpredicted. For calculating the RMSEs of the simulated longitudinal velocity profiles in the developing, fully developed, and recovering regions, the locations were selected at $X/Y_1 = 12$, 36, and 105 from the gate, respectively. According to the measurements by Long et al. [9], all velocity profiles were taken in the plane at $z/W = 0.36$ mm or $z/W = 168$ mm from the channel wall. According to the RMSEs in Table 4, the longitudinal velocity profile in

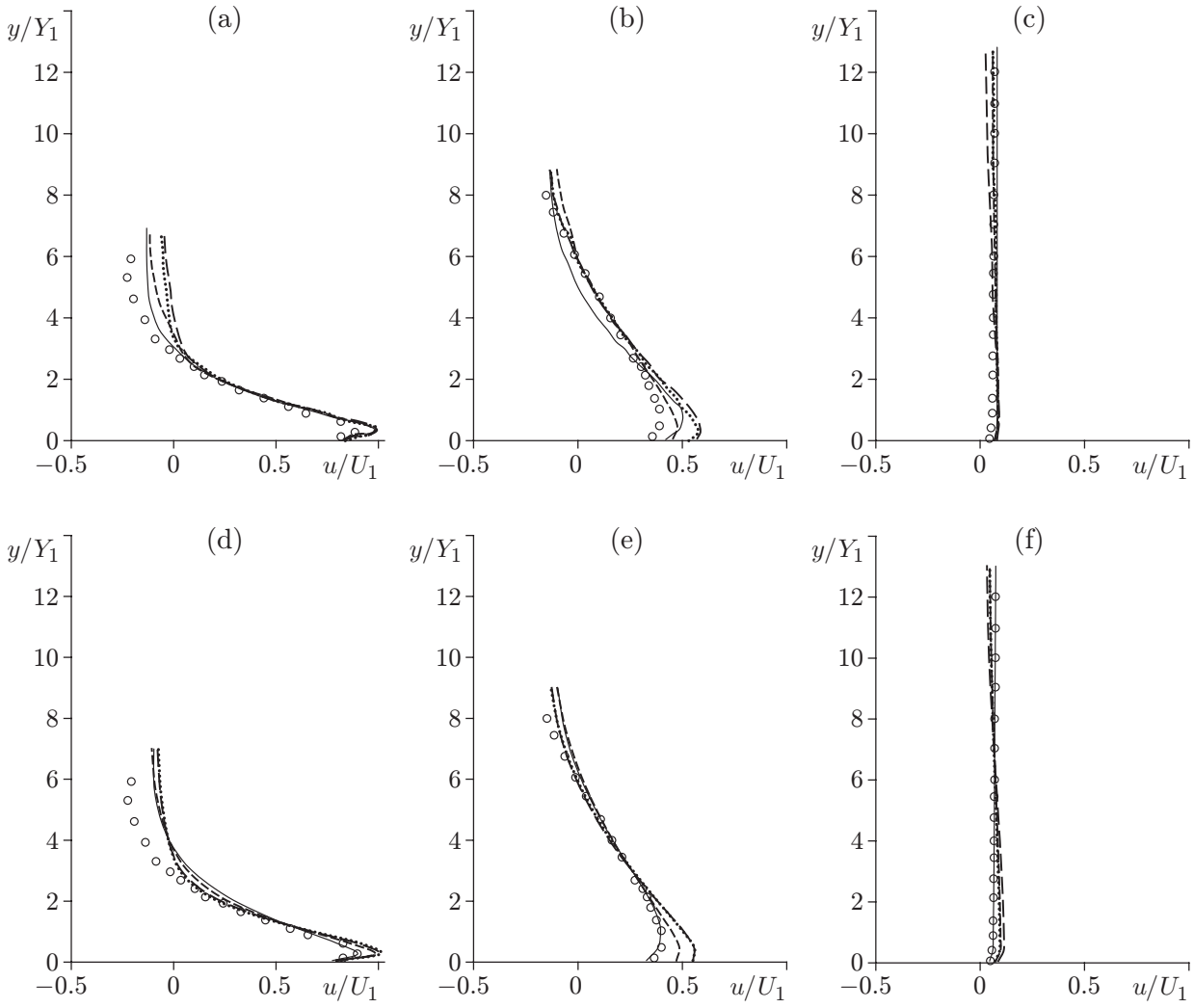

Fig. 2. Calculated (curves) and experimental (points) longitudinal velocity profiles: simulations by the standard wall functions (a–c) and simulations by the enhanced wall treatment (d–f) for $x/Y_1 = 12$ (a and d), 36 (b and e), and 105 (c and f); other notations the same as in Fig. 1.

the developing region simulated by the RSM turbulence model with the standard wall functions is more accurate than those predicted by the other methods. In the fully developed region, the longitudinal velocity simulated by the RSM turbulence model with the enhanced wall treatment exhibits better agreement with the experimental values. In the wall jet region, the flow is influenced by the boundary layer characteristics [15]. The velocities simulated by the enhanced wall treatment method and different turbulent models is in better agreement with the experimental results that those obtained by using the standard wall functions (see Table 4).

In the recovering region, the velocity distribution is almost uniform over the channel depth, and the agreement between the numerical and experimental values is good. The RSM predictions with both near wall treatments are more accurate than the predictions of the other turbulence models (see Fig. 2 and Table 4). For the simulated longitudinal velocity profiles, the results of the standard and RNG k–ε models with enhanced wall treatment are similar to each other. A comparison between the measured and simulated maximum mean velocity of experiment Nos. 3, 6, and 8 shows that the simulated results of the RSM and standard k–ε models generally have good agreement with the experimental data. With increasing Froude number, the simulation results of the RSM model show better agreement with the experimental results than the standard k–ε model.

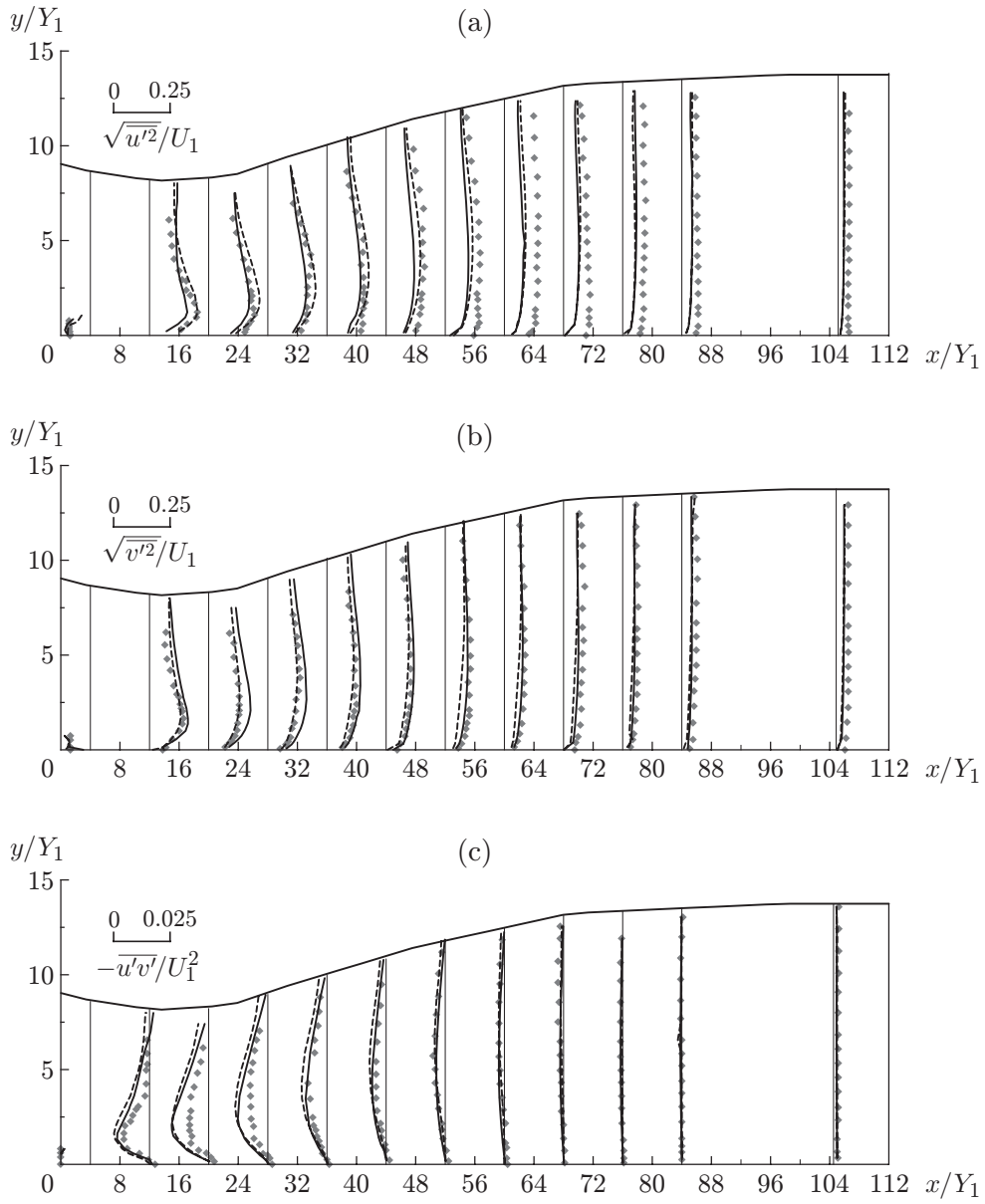

Fig. 3. Experimental (points) and calculated (curves) turbulence intensity $\sqrt{\overline{u'^2}}$ (a) and $\sqrt{\overline{v'^2}}$ (b) and turbulent shear stress $-\overline{u'v'}$ (c): the solid and dashed curves show the results calculated by the standard k–ε model and RSM; the points are the experimental data [9].

Table 4. Relative root-mean-square error of the simulated longitudinal velocity profiles

Near-wall treatment approach	Turbulence model	Δ, %		
		$x/Y_1 = 12$	$x/Y_1 = 36$	$x/Y_1 = 105$
Standard near-wall functions	RSM	16.3	18.9	5.4
	RNG k–ε model	29.5	24.4	6.4
	Realizable k–ε model	34.1	28.3	8.7
	Standard k–ε model	24.2	14.1	7.5
Enhanced wall treatment	RSM	25.1	9.2	5.3
	RNG k–ε model	26.6	20.2	6.4
	Realizable k–ε model	29.1	23.3	10.6
	Standard k–ε model	22.2	12.2	6.4

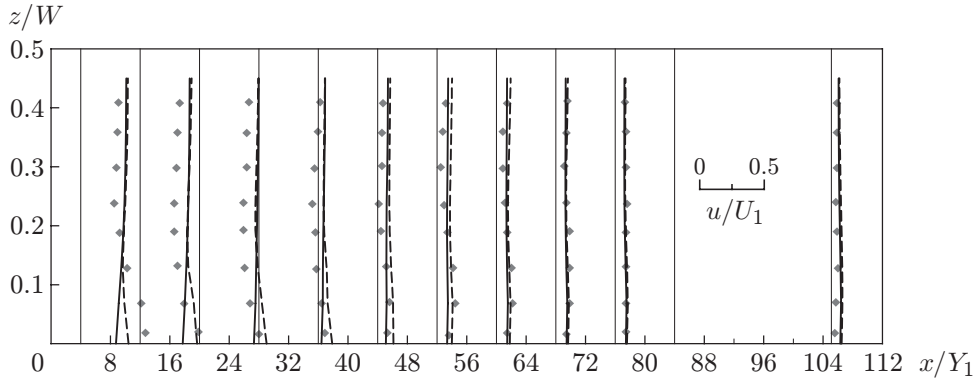

Fig. 4. Experimental (points) and calculated (curves) longitudinal velocity profiles across the channel: the solid and dashed curves show the results simulated by the standard k–ε model and RSM, respectively; the points are the experimental data [9].

The longitudinal turbulence intensity $\sqrt{\overline{u'^2}}$ and the values of $\sqrt{\overline{u'^2}}$ simulated by the standard k–ε and RSM turbulence models are compared with the experimental results (Fig. 3a). With increasing distance from the gate, the longitudinal turbulence intensity rapidly decreases. The RSM results in the wall jet region near the channel bed show better agreement with the experimental results than the standard k–ε model. The corresponding results of the other turbulence models are underpredicted behind the roller region. The vertical turbulence intensity $\sqrt{\overline{v'^2}}$ simulated by the RSM model is more accurate than the results of the standard k–ε model in the wall jet and recirculation region. Behind these regions, the RSM underpredicts the values of $\sqrt{\overline{v'^2}}$, while the standard k–ε model results show good agreement with the experimental data (Fig. 3b). A comparison between the results of the RSM turbulence model with the experimental results shows that the RSM model overpredicts the turbulent shear stress $-\overline{u'v'}$ in the recirculation region. At the beginning of this region, the standard k–ε model is more accurate than the RSM model. However, downstream of the recirculation region, the results of the turbulence models shows good agreement with the experimental results (Fig. 3c).

The simulated longitudinal velocity distributions across the channel ($y/Y_1 = 5.3$) are compared with the experimental data in experiment No. 8 (Fig. 4). According to Fig. 4, the longitudinal velocities simulated by the standard k–ε and RSM models are overpredicted near the symmetry plane in the roller region. In the wall jet region near the side wall, the values of u are underpredicted by the turbulence models; at a large distance from the gate, the RSM results are overpredicted, while the results of the standard k–ε model show general agreement with the experimental results. In the recovering region, the turbulence models predict similar results and show good agreement with the experimental data. The differences between the experimental and numerical results in the roller region in the plane $y/Y_1 = 5.3$ are most likely due to the extreme complexity of the flow.

The longitudinal velocity and the turbulent shear stress $\overline{u'v'}$ of experiment No. 6 simulated by using the standard k–ε and RSM turbulence models are compared with the experimental results at four locations of three cross sections at $x/Y_1 = 4$, 32, and 64. In the presence of the vertically vortex motion near the gate opening on the water

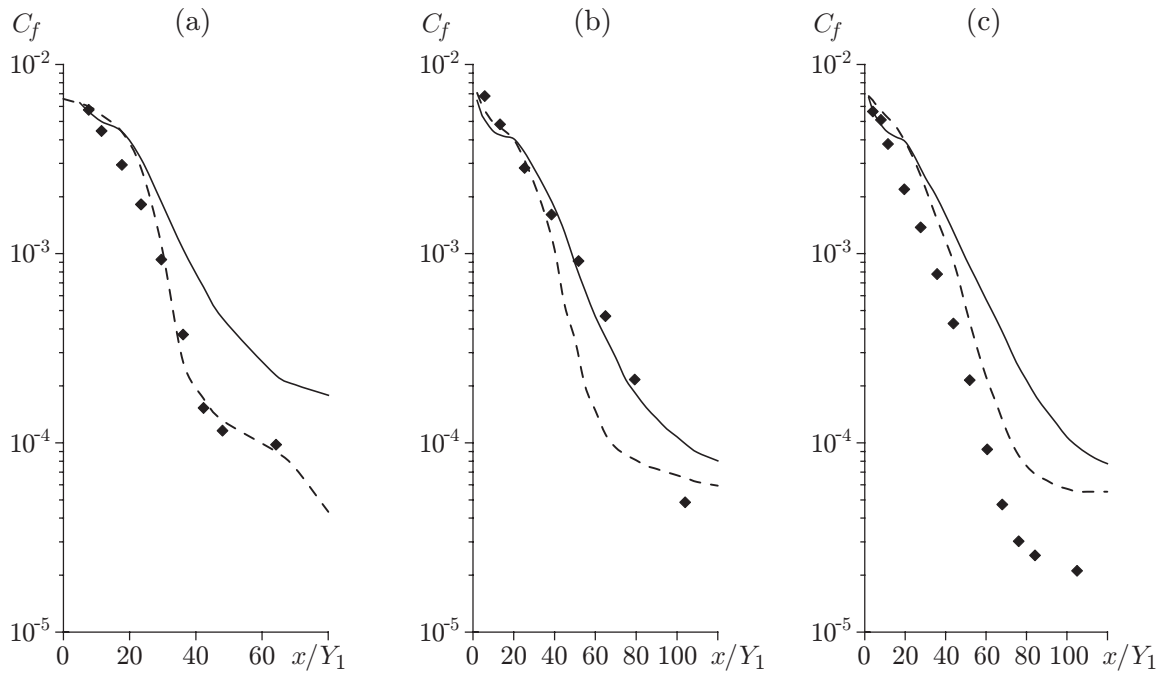

Fig. 5. Experimental (points) and calculated (curves) values of the shear stress coefficient on the channel bed: the points are the experimental points [9] [(a) experiment No. 3; (b) experiment No. 6; (c) experiment No. 8]; the solid and dashed curves show the results simulated by the standard k–ε model and RSM, respectively.

surface, the effect of the reversing flow near the center plane of the channel is higher than near the side walls [9]. The agreement of the numerical and experimental results for the longitudinal velocity is good in the wall jet region. In the reverse flow region, the numerical results for the longitudinal velocity are underpredicted near the side wall and overpredicted near the symmetry plane, while they show general agreement at $z/W = 0.24$. At $x/Y_1 = 32$, the results of the turbulence models agree well with the experimental results, but the RSM model accuracy is higher than the accuracy of the standard k–ε model near the symmetry plane and side wall. At $x/Y_1 = 64$, the simulation results of the RSM model show better agreement with the experimental results than those predicted by the standard k–ε model. The simulated turbulent shear stress has good agreement with the experimental values in the wall jet region, and the results of both turbulent models are approximately similar. At $x/Y_1 = 32$, the agreement between the numerical and experimental values is excellent near the channel bed. Above the wall region, the simulated turbulent shear stress is overpredicted near the side wall and underpredicted near the symmetry plane of the channel, although the simulated turbulent shear stress is in general agreement with the experimental results at $z/W = 0.13$ and 0.24. At $x/Y_1 = 64$, the results of the RSM model are more accurate than those of the standard k–ε model near the side wall of the channel.

The measured and simulated bed shear stress coefficients of experiment Nos. 3, 6, and 8 are compared in Fig. 5. The shear stress coefficient can be defined as

$$C_f = \frac{\tau_w}{\rho U_{\text{in}}^2/2} = \frac{u_*^2}{U_{\text{in}}^2/2},$$

where τ_w and u_* are the bed shear stress and shear velocity, respectively. As shown in Fig. 5, the agreement between the numerical and experimental results for the shear stress coefficient is good, although the shear stress coefficient predicted by the standard k–ε model is generally higher than the results of the RSM model.

CONCLUSIONS

Three-dimensional submerged hydraulic jumps are numerically investigated in this study. The VOF method and different turbulence models, such as RSM, standard k–ε, RNG k–ε, and realizable k–ε models, are used to predict the free surface and turbulence structure of the submerged hydraulic jumps. The performance of the turbulence models is also studied by the standard wall functions and enhanced wall treatment methods. The numerical results of the three-dimensional submerged hydraulic jumps are in acceptable agreement with the experimental data.

The RNG k–ε turbulence model with the enhanced wall treatment method provide the highest accuracy in the water surface simulation. Near the channel bed of the fully developed region, the RSM model with the enhanced wall treatment method shows better agreement with the experimental longitudinal velocity than the other turbulence models. The standard k–ε model is more accurate in the longitudinal velocity prediction than the RNG and realizable k–ε models. In the roller region, the longitudinal velocity distributions across the channel are underpredicted by the RSM and standard k–ε models. Generally, the standard k–ε model simulates the shear stress coefficient and the maximum mean velocity of the submerged hydraulic jumps more adequately than the RSM. The longitudinal and vertical turbulence intensity and turbulence shear stress simulated by the RSM and standard k–ε model are in good agreement with the experimental data.

REFERENCES

1. D. Long, P. M. Steffler, N. Rajaratnam, and P. Smy, "Structure of Flow in Hydraulic Jumps," J. Hydraul. Res. **29** (2), 207–218 (1990).
2. M. Liu, N. Rajaratnam, and D. Zhu, "Turbulence Structure of Hydraulic Jumps of Low Froude Numbers," J. Hydraul. Eng. Proc. ASCE **130**, 511–520 (2004).
3. J. A. McCorquodale, "Hydraulic Jumps and Internal Flows," in *Encyclopedia of Fluid Mechanics*, Ed. by N. P. Cheremisinoff (Gulf, Houston, 1986), Vol. 2, Chapter 6, pp. 120–173.
4. H. Rouse, T. T. Siao, and S. Nagaratnam, "Turbulence Characteristics of the Hydraulic Jumps," J. Hydraul. Div. Proc. ASCE **84** (1), 1–30 (1958).
5. I. A. Svendsen, J. Veeramony, J. Bakunin, and J. T. Kirby, "The Flow in Weak Turbulent Hydraulic Jump," J. Fluid Mech. **418**, 25–57 (2000).
6. N. S. G. Rao and N. Rajaratnam, "The Submerged Hydraulic Jump," J. Hydraul. Div. Proc. ASCE **89** (HY1), 139–162 (1963).
7. N. Rajaratnam, "The Hydraulic Jump as a Wall Jet," J. Hydraul. Div. Proc. ASCE **91** (5), 107–132 (1965).
8. S. Wu and N. Rajaratnam, "Free Jumps, Submerged Jumps and Wall Jets," J. Hydraul. Res. **33** (2), 197–212 (1995).
9. D. Long, P. M. Steffler, and N. Rajaratnam, "LDA Study of Flow Structure in Submerged Hydraulic Jumps," J. Hydraul. Res. **28** (4), 437–460 (1990).
10. I. Ohtsu, Y. Yasuda, and M. Ishikawa, "Submerged Hydraulic Jumps Below Abrupt Expansions," J. Hydraul. Eng. Proc. ASCE **125** (5), 492–499 (1999).
11. S. Dey and A. Sarkar, "Characteristics of Turbulent Flow in Submerged Jumps on Rough Beds," J. Eng. Mech. Proc. ASCE **134** (1), 49–59 (2008).
12. D. Long, P. M. Steffler, and N. Rajaratnam, "A Numerical Study of Submerged Hydraulic Jumps," J. Hydraul. Res. **29** (3), 293–308 (1991).
13. A. M. Gharangik and M. H. Chaudhry, "Numerical Model of Hydraulic Jump," J. Hydraul. Eng. Proc. ASCE **117**, 1195–1209 (1991).
14. S. Chippada, B. Ramaswamy, and M. F. Wheeler, "Numerical Simulation of Hydraulic Jump," Int. J. Numer. Methods Engng. **37**, 1381–1397 (1994).
15. F. Ma, Y. Hou, and P. Prinos, "Numerical Calculation of Submerged Hydraulic Jump," J. Hydraul. Res. **39** (5), 1–11 (2002).
16. C. W. Hirt and B. D. Nicholls, "Volume of Fluid (VOF) Method for Dynamics of Free Boundaries," J. Comput. Phys. **39**, 201–221 (1981).
17. M. A. Sarker and D. G. Rhodes, "Physical Modeling and CFD Applied to Hydraulic Jumps," Report of Cranfield Univ. (2002).
18. Q. Zhao, S. K. Misra, S. Svendsen, and I. Kirby, "Numerical Study of a Turbulent Hydraulic Jump," in *Proc. of 17th Eng. Mech. Conf.* (Univ. of Delaware, New York, 2004).

19. A. Gonzalez and F. Bombardelli, "Two-Phase Flow Theory and Numerical Models for Hydraulic Jumps, Including Air Entrainment," in *Proc. of the 31st IAHR Congress* (Seoul, Korea, 2005).
20. B. E. Launder and D. B. Spalding, "The Numerical Computation of Turbulent Flows," Comput. Methods Appl. Mech. Eng. **3**, 269–289 (1974).
21. H. C. Chen and V. C. Patel, "Near-Wall Turbulence Models for Complex Flows Including Separation," AIAA J. **26** (6), 641–648 (1988).
22. T. Jongen, "Simulation and Modeling of Turbulent Incompressible Flows," Thesis Ph.D. (Lausanne, 1992).
23. B. Kader, "Temperature and Concentration Profiles in Fully Turbulent Boundary Layers," Int. J. Heat Mass Transfer **24** (9), 1541–1544 (1981).
24. M. Wolfstein, "The Velocity and Temperature Distribution of One-Dimensional Flow with Turbulence Augmentation and Pressure Gradient," Int. J. Heat Mass Transfer **12**, 301–318 (1969).
25. T. H. Shih and J. L. Lumley, "Kolmogorov Behavior of Near-Wall Turbulence and its Application in Turbulence Modeling," Int. J. Comput. Fluid Dyn. **1** (1), 43–56 (1993).
26. H. D. Pasinato, "Some Results Based on Near-Wall Turbulence," Int. J. Comput. Fluid Dyn. **14** (2), 159–169 (2000).
27. J. Y. Kim, A. J. Ghajar, C. Tang, and G. L. Foutch, "Comparison of Near-Wall Treatment Methods for High Reynolds Number Backward-Facing Step Flow," Int. J. Comput. Fluid Dyn. **19** (7), 493–500 (2005).